Simulation of Stand-to-Sit Biomechanics for Robotic Exoskeletons and Prostheses with Energy Regeneration

Brokoslaw Laschowski, *Student Member, IEEE*, Reza Sharif Razavian, and John McPhee

***Abstract* — Previous studies of robotic exoskeletons and prostheses with regenerative actuators have focused exclusively on level-ground walking applications. Here we analyzed the lower-limb joint mechanical power during stand-to-sit movements using inverse dynamic simulations to estimate the biomechanical energy available for electrical regeneration. Nine subjects performed 20 sitting and standing movements while lower-limb kinematics and ground reaction forces were measured. Subject-specific body segment parameters were estimated using system parameter identification. Joint mechanical power was calculated from net joint torques and rotational velocities and numerically integrated over time to estimate the joint biomechanical energy. The hip absorbed the largest peak negative mechanical power (1.8 ± 0.5 W/kg), followed by the knee (0.8 ± 0.3 W/kg) and ankle (0.2 ± 0.1 W/kg). Negative mechanical work on the hip, knee, and ankle joints per stand-to-sit movement were 0.35 ± 0.06 J/kg, 0.15 ± 0.08 J/kg, and 0.02 ± 0.01 J/kg, respectively. Assuming known regenerative actuator efficiencies (i.e., maximum 63%), robotic exoskeletons and prostheses could theoretically regenerate ~26 Joules of electrical energy while sitting down, compared to ~19 Joules per walking stride. Given that these regeneration performance calculations are based on healthy young adults, future research should include seniors and/or rehabilitation patients to better estimate the biomechanical energy available for electrical regeneration.**

***Index Terms* — biomechanics; efficiency; exoskeletons; prosthetics; wearable robotics**

I. Introduction

OVER 12 million people in the United States alone have mobility impairments resulting from stroke, spinal cord injury, and other neuromusculoskeletal conditions [1]. There are ~2 million Americans with limb amputations [2]. These numbers are expected to increase with the aging population and growing incidences of cancer and diabetes [1]-[3]. Fortunately, robotic exoskeletons and prostheses can help mobility-impaired individuals to perform movements that involve net positive mechanical work (e.g., sit-to-stand) by mimicking their amputated or unimpaired biological muscles [4]-[9]. However, these robotic assistive technologies typically require significant electrical power and large onboard batteries to facilitate daily functioning [5]-[6], [10]-[11]. For instance, most robotic knee prostheses under research and development consume 43 ± 30 W of electricity during level-ground walking; provide only 3.1 ± 2.2 hours of maximum operation; and weigh 4.0 ± 1.1 kg [4], [6]. Similarly, most robotic lower-limb exoskeletons provide only 1-5 hours of maximum operation [1]. Portable electricity has been considered one of the leading challenges to developing robotic exoskeletons for real-world environments [1], [10]-[11]. Barring advances in energy storage devices, research into energy-efficient biomechatronic design and control systems is warranted.

Energy regeneration is a potential solution to the aforementioned shortcomings. Human joints can provide both negative mechanical power (braking) and positive mechanical power (motoring) [12]. During level-ground walking, the knee joint resembles a damper mechanism, performing net negative mechanical work via energy dissipation, and the ankle joint resembles an actuating motor, performing net positive mechanical work and generating forward propulsion [5], [10]-[12]. These human walking biomechanics are illustrated in Fig. 1. Similar to regenerative braking in electric and hybrid electric vehicles [13]-[14], several robotic exoskeletons and prostheses have used regenerative actuators to convert the otherwise dissipated joint biomechanical energy during negative work movements into electrical energy by reversing the direction of operation [5], [15]-[30]. Such bidirectional power flow during motoring and generating operations requires backdriveable actuator-transmission systems with low mechanical impedance [31]-[36]. These energy-efficient powertrains can allow for lighter onboard batteries and/or extend the operating durations between recharging. Decreasing the onboard battery weight can also help minimize 1) the metabolic power consumption during walking, and 2) discomfort from excessive tugging on the human-prosthesis interface [2].

B. Laschowski is with the Department of Systems Design Engineering at the University of Waterloo, Waterloo, Canada (e-mail: blaschow@uwaterloo.ca).

R.S. Razavian is with the Department of Biology at Northeastern University, Boston, USA (e-mail: r.sharifrazavian@northeastern.edu).

J. McPhee is with the Department of Systems Design Engineering at the University of Waterloo, Waterloo, Canada (e-mail: mcphee@uwaterloo.ca).

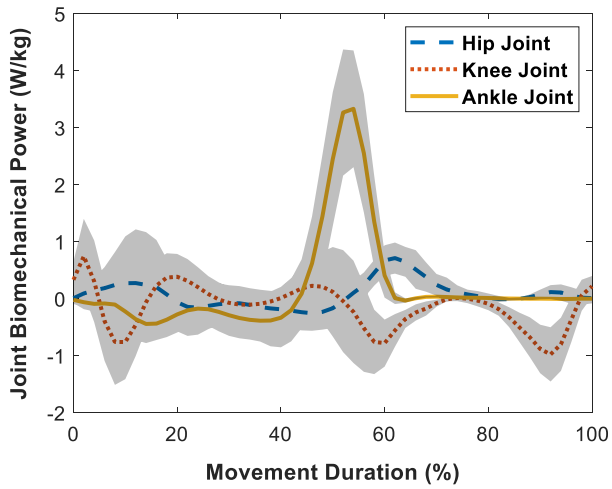

Fig. 1 Hip, knee, and ankle joint mechanical power per walking stride, normalized to total body mass. Data were taken from Winter [12]. The uncertainties are ± one standard deviation across different subjects (n=19). The trajectories begin and end with heel-strike.

Previous studies of robotic exoskeletons and prostheses with regenerative actuators have focused exclusively on level-ground walking applications [15]-[30], [33], [37]-[39]. However, prospective users of these assistive technologies typically walk slower (e.g., ~24% reduction from 25 to 75 years age) and take fewer steps/day (e.g., ~75% reduction from 60 to 85 years age) [3], therein limiting the potential for electrical regeneration from level-ground walking. In contrast, sitting and standing movements are considered more applicable daily activities of mobility-impaired individuals [3]. For reference, healthy young adults perform ~60 sitting and standing movements each day [40]. Although several robotic exoskeletons and prostheses have been designed and evaluated for sitting and standing movements [7]-[9], [40]-[46], these devices did not include regenerative actuators. Regenerating energy while sitting down represents an unexplored and potentially viable method to supplementing that from level-ground walking. Motivated to find new opportunities for energy savings, we analyzed the lower-limb joint mechanical power during stand-to-sit movements using inverse dynamic simulations to estimate the biomechanical energy available for electrical regeneration.

II. Methods

A. Motion Capture Experiments

Nine subjects were recruited and provided informed written consent (height: 180 ± 4 cm, body mass: 78 ± 7 kg, age: 25 ± 3 years, sex: male). Each subject performed 20 sitting and standing movements while lower-limb kinematics and ground reaction forces were measured using motion capture cameras and force plates, respectively (see Fig. 2). Different force plates were used to experimentally measure the ground reaction forces underneath the seat and feet. The seat height was ~46 cm. The motion capture cameras (Optotrak, Northern Digital Incorporation, Canada) provided 3D measurements of active marker positions in global coordinates. Active marker systems are generally considered the gold standard in human movement biomechanics [47]. The motion capture cameras and force plates were sampled at 100 Hz and 300 Hz, respectively. For tracking individual body segment positions in the sagittal plane, virtual markers were digitized overlying palpable anatomical landmarks on the right lower-limb, including the lateral malleolus, lateral femoral and tibial condyles, and greater trochanter. These marker positions correspond with those recommended by the International Society of Biomechanics [47]. This research study was approved by the University of Waterloo Office of Research Ethics.

B. Data Processing

Missing marker data were estimated using cubic spline interpolations. The ankle and hip joint centers were assumed at the lateral malleolus and greater trochanter markers, respectively. The estimated knee joint center was the midpoint between the lateral femoral and tibial condyle markers [47]. Piecewise cubic Hermite interpolating polynomials were used to resample and time-normalize the kinematic measurements. Average line vectors between the ankle and knee joint centers, and knee and hip joint centers, defined the shank and thigh body segment lengths, respectively. Inverse kinematics converted the marker positions to joint coordinates through vector algebra. The ankle angle was the angle between the shank and horizontal axis (see Fig. 3). The relative angle between the shank and thigh segments defined the knee angle. Given the relative rotations between the pelvis and head-arms-trunk (HAT) segment, the measured pelvis marker-cluster rotations differed from HAT segment rotations. Therefore, the HAT segment was assumed vertical when standing (initial posture) and seated (final posture) and the pelvis angle rotations were assumed to progress linearly throughout the movement. The relative angle between the thigh and HAT segments defined the hip angle. Joint angles were filtered using a 10th-order low-pass Butterworth filter with 5 Hz cut-off

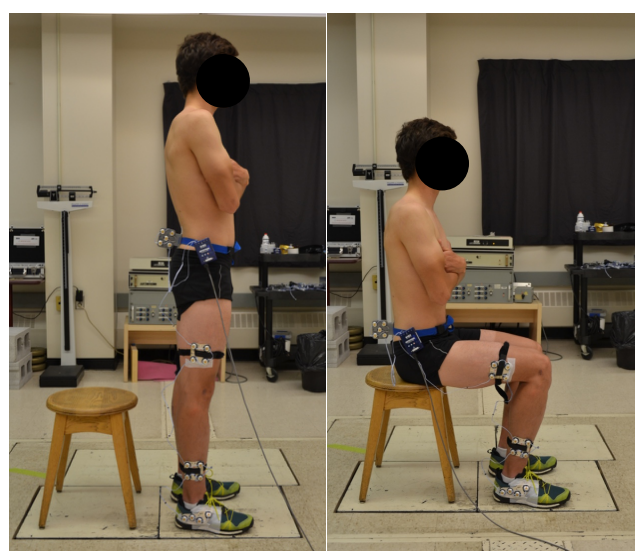

Fig. 2 Photographs of the biomechanical measurements of stand-to-sit movements with motion capture cameras and force plates.

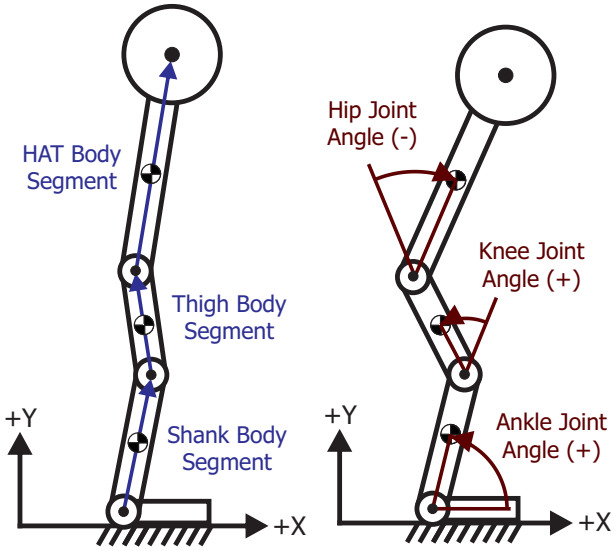

Fig. 3 2D human biomechanical model including hip, knee, and ankle joints and HAT, thigh, and shank body segments.

frequency and zero-phase digital filtering [12]. The joint rotational speeds and accelerations were calculated by numerically differentiating the joint angles.

Similar to previous research [41], the pelvis translational velocities, which were estimated from the marker-cluster shown in Fig. 2, were used to segment the sitting and standing movement durations. These kinematic measurements were filtered using a 10th-order low-pass Butterworth filter with 3 Hz cut-off frequency, and zero-phase digital filtering and moving average smoothing filtering. The sitting and standing movement durations were segmented when the pelvis translational velocities exceeded a percentage of their maximum values, which were estimated through trial-and-error simulations. The force plate measurements were filtered using a 10th-order low-pass Butterworth filter with 30 Hz cut-off frequency, and zero-phase digital filtering. Piecewise cubic Hermite interpolating polynomials were used to time-normalize the force plate measurements.

C. *Biomechanical Model Design*

The human biomechanical system was dynamically modelled using MapleSim (Maplesoft, Canada). The biomechanical model comprised a 2D sagittal-plane, inverted triple-pendulum with shank, thigh, and HAT rigid body segments (see Fig. 3). Since the foot marker position remained relatively unchanged throughout the sitting and standing movements (i.e., maximum horizontal and vertical displacements of ~1.27 cm and ~0.7 cm, respectively), the foot segment was modelled as fixed to the ground. The ankle, knee, and hip were modelled as revolute joints. Biological passive joint torques, including stiffness and damping, were ignored since we assumed ideal joints for modelling an exoskeleton or prosthetic system. The biomechanical model had three degrees-of-freedom and was mathematically represented by three generalized coordinates with zero algebraic constraints. Assuming the foot segment was fixed to the ground and had relatively small mass, the ground reaction forces underneath the feet corresponded with the ankle joint reaction forces, and the ground reaction moments were offset by the ankle position relative to the center of pressure (COP). The measured ground reaction forces underneath the seat were applied to the biomechanical model buttocks when seated. MapleSim automatically generated the multibody system equations symbolically using linear graph theory, therein enabling computationally efficient dynamic simulations.

D. *Simulation and Parameter Identification*

The biomechanical model was driven using the experimental joint kinematics and seat forces. The ankle, knee, and hip joint torques (τ), and the ground reaction forces and moment underneath the feet, were calculated from inverse dynamics. In conventional "bottom-up" inverse dynamics, the joint reaction forces and torques are solved segment-by-segment (i.e., starting from ground and moving sequentially upward). Therefore, the calculated forces and accelerations on the final body segment (HAT) do not satisfy the dynamic equations because of errors in kinematics, system parameters, and/or unmodeled dynamics [48]-[49]. In contrast, our biomechanical model was driven using the measured joint kinematics in a multibody dynamics simulation and therefore can be considered more dynamically consistent. Specifically, the simulated ground reaction forces from inverse dynamics were compared with those experimentally measured, and the body segment inertial parameters were concurrently optimized to minimize the differences. Although human body segment parameters can be estimated using medical imaging [50]-[51] and/or anthropometric proportions from cadaver research [52], we used system parameter identification for better dynamical consistency. The parameter identification involved using constrained nonlinear programming (Fmincon, MATLAB) and an interior-point algorithm to estimate the subject-specific body inertial segment parameters (i.e., mass, center of mass, and moment of inertia). The optimization searched for the parameters that minimized the sum of squared differences in the ground reaction forces (GRF) and moments (GRM) between the experimental measurements (m) and inverse dynamic simulations (s) at each time step (i). The optimization multiobjective cost function was:

$$J = \sum_i w_1 (GRF_m[i] - GRF_s[i])^2 \times \frac{1}{(BM)^2} + \sum_i w_2 \left((GRM_m[i] + GRM_{offset}) - GRM_s[i]\right)^2 \times \frac{1}{(H \times BM)^2} \quad (1)$$

where the two-dimensional GRF vector included both the horizontal (GRF_x) and vertical (GRF_y) components, the GRM was around the z-axis, BM was body mass, coefficient H = 1 meter, and GRM_{offset} compensated for the distance between the ankle and foot center of pressure according to {$GRM_{offset} = GRF_y \times COP_x - GRF_x \times COP_y$} with COP_x and COP_y being the estimated average positions of the foot center of pressure relative to the ankle joint. The optimization variables were the shank, thigh, and HAT segment mass, center of mass, and moment of inertia. Other variables included "$seat_{offset}$" and the COP_x. $Seat_{offset}$ was the distance between the biomechanical model buttocks (i.e., vertical seat force point-of-application) and the hip

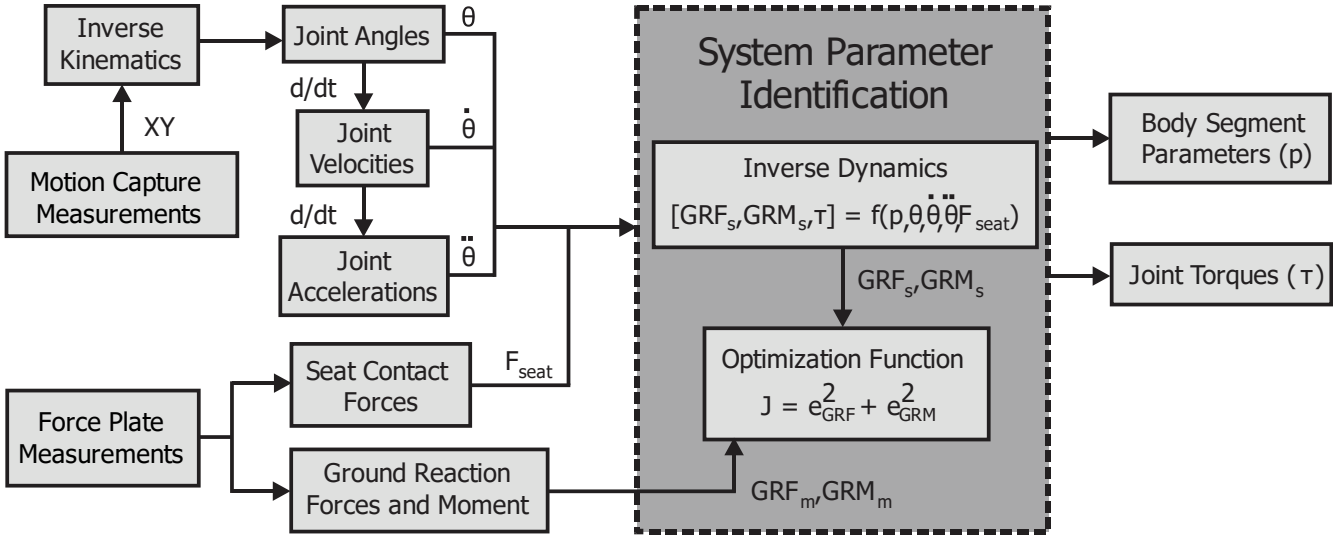

Fig. 4 Flow diagram of the experimental and computational methods, including the biomechanical measurements, inverse kinematic and dynamic analyses, and system parameter identification. The nomenclatures are defined in the text.

joint center. The COP position moved underneath the base of support. However, the ground reaction forces were not used to drive the biomechanical model but rather to validate the system identification. The best average position (denoted as parameter COP_x in the optimization) was found using our system parameter identification. The COP_y was the ankle marker height. The optimization was constrained by setting 1) lower and upper bounds on the individual variables, and 2) the sum body segment masses equaled to the measured total body mass. Initial guesses were taken from human anthropometrics and/or were the midpoints between the upper and lower bounds. Each term in the optimization had equal weights. The stopping criteria for the step size and objective function changes were both 1e-8 between iterations. Our experimental and computational methods are summarized in Fig. 4. Once the optimal system parameters were found, the joint mechanical power was calculated from net joint torques and rotational speeds ($P_J = \tau_J \cdot \dot{\theta}_J$) and numerically integrated over time to estimate the joint biomechanical energy.

III. Results

The movement trajectories were time-normalized to facilitate between and within subject averaging. Fig. 5 shows the calculated hip, knee, and ankle joint angles during the stand-to-sit movements from the inverse kinematics analysis. Note that decreasing joint angles represented hip flexion, knee extension, and ankle dorsiflexion, while increasing joint angles represented hip extension, knee flexion, and ankle plantar flexion. The uncertainties are ± one standard deviation across each subject (n=9) and trial (20 trials/subject), therein amounting to 180 total trials. There were minor variations in the joint kinematics between and within subjects, as demonstrated by the small standard deviations.

Fig. 6 shows the calculated hip, knee, and ankle joint torques from the inverse dynamic simulations; the corresponding peak values were 0.7 ± 0.1 Nm/kg, 1.1 ± 0.3 Nm/kg, and 0.4 ± 0.1 Nm/kg. The calculated hip, knee, and ankle joint mechanical power while sitting down are shown in Fig. 7. The hip produced the largest peak negative mechanical power (1.8 ± 0.5 W/kg), followed by the knee (0.8 ± 0.3 W/kg) and ankle (0.2 ± 0.1 W/kg). Negative mechanical work from the hip, knee, and ankle joints per stand-to-sit movement were 0.35 ± 0.06 J/kg, 0.15 ± 0.08 J/kg, and 0.02 ± 0.01 J/kg, respectively. Subjective feedback from participants indicated that performing stand-to-sit movements were significantly more challenging than sit-to-stand movements, particularly from a balance control perspective. The experimental and simulated biomechanical data were uploaded to IEEE DataPort and are publicly available for download at https://ieee-dataport.org/documents/measurement-and-simulation-human-sitting-and-standing-movement-biomechanics. Prospective users of the biomechanical dataset are requested to reference this paper.

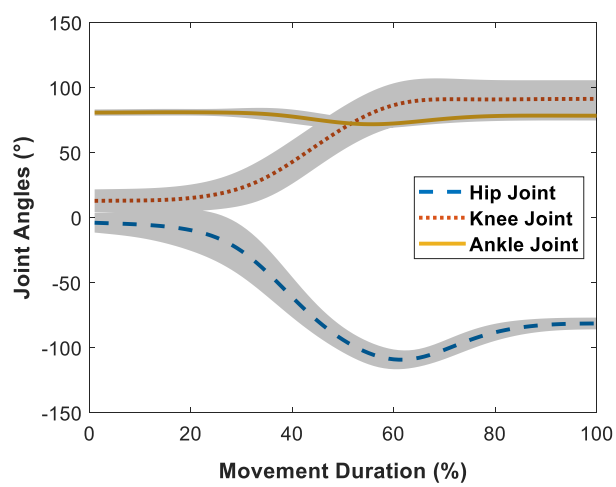

Fig. 5 Hip, knee, and ankle joint angles during stand-to-sit movements from inverse kinematics. The uncertainties are ± one standard deviation across different subjects (n=9) and trials (20 trials/subject).

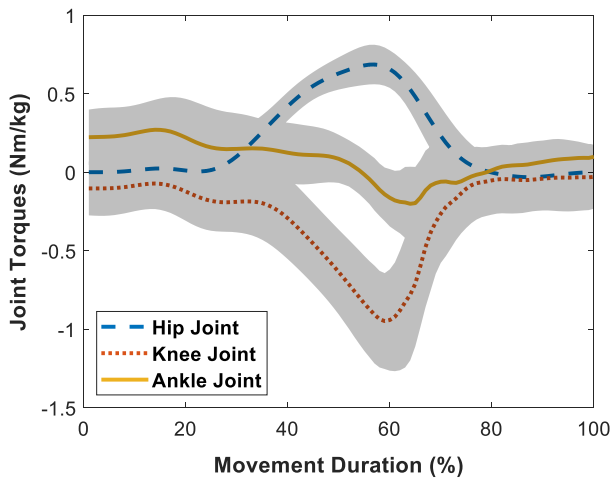

Fig. 6 Hip, knee, and ankle joint torques during stand-to-sit movements from inverse dynamics, normalized to total body mass. The uncertainties are ± one standard deviation across different subjects (n=9) and trials (20 trials/subject).

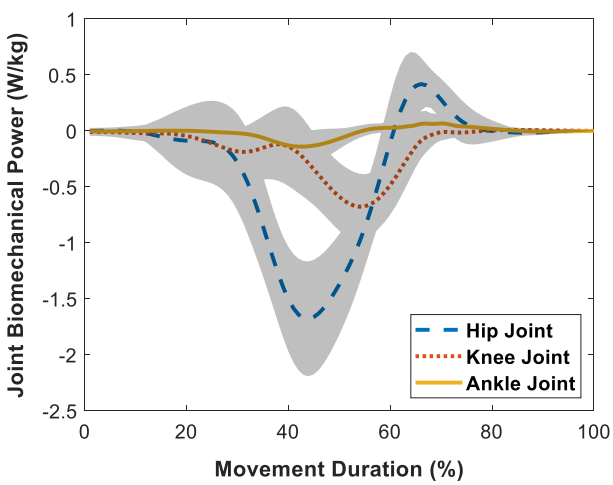

Fig. 7 Hip, knee, and ankle joint mechanical power during stand-to-sit movements, normalized to total body mass. The uncertainties are ± one standard deviation across different subjects (n=9) and trials (20 trials/subject).

IV. Discussion

Regenerative actuators can improve the energy-efficiency and extend the operating durations of robotic exoskeletons and prostheses by converting the otherwise dissipated joint biomechanical energy during negative work movements into electrical energy for battery recharging, hence the term regenerative braking. However, these energy-efficient powertrains have been exclusively designed and evaluated for level-ground walking applications [15]-[30], [33], [37]-[39]. Building on previous research, we analyzed the lower-limb joint mechanical power during stand-to-sit movements using inverse dynamic simulations to estimate the biomechanical energy available for electrical regeneration during locomotor activities considered more applicable to aging and rehabilitation populations [3] (e.g., some individuals with severe mobility impairments perform no locomotor activities other than sit-to-stand and stand-to sit movements for wheelchair transfers).

The simulated peak negative mechanical power from the hip, knee, and ankle joints were 1.8 ± 0.5 W/kg, 0.8 ± 0.3 W/kg, and 0.2 ± 0.1 W/kg, respectively. In comparison, previous experimental measurements with robotic prostheses reported 0.7-0.8 W/kg peak knee joint mechanical power during sitting and standing movements [40], [45]. The strong quantitative agreement between the simulated (0.8 ± 0.3 W/kg) and experimental (0.7-0.8 W/kg) [40], [45] peak knee joint mechanical powers supported the model validation. The model validation was further corroborated by relatively good agreements in peak knee joint torques between our biomechanical simulations (1.1 ± 0.3 Nm/kg) and previous experimental research on robotic exoskeletons and prostheses for sitting and standing movements (0.8-1.0 Nm/kg) [40],[42]-[44]. Note that these joint torques are high enough to dynamically backdrive an actuator-transmission system (e.g., requiring 1-3 Nm backdrive torque) [32]-[34], [36] and therefore capable of regenerating electrical energy while sitting down.

The hip performed the most negative mechanical work during stand-to-sit movements (0.35 ± 0.06 J/kg), followed by the knee (0.15 ± 0.08 J/kg) and ankle (0.02 ± 0.01 J/kg). Although the hip performed the most negative mechanical work, and therefore has the greatest potential for electrical regeneration, most robotic exoskeletons and prostheses with regenerative actuators have focused on knee-centered designs [15]-[20], [22]-[30], [33], [37]-[39]. Fig. 8 shows our regenerative powertrain system model. A standard electric motor converts electrical power (VI) to mechanical power ($\tau\dot{\theta}$). However, when backdriven, the motor operates like an electric generator, converting mechanical power to electrical power. Regenerative actuator efficiency (η) is defined as the percentage of mechanical-to-electrical power conversion. Assuming an 80-kg user and known regenerative actuator efficiencies (η = maximum 63%) [19], [25]-[26], [53]-[54], robotic exoskeletons or prostheses could theoretically regenerate ~26 Joules of total electrical energy while sitting down. Backdriving the same regenerative actuator using Winter's walking data [12], ~19 Joules of electrical energy could be regenerated per stride. Note that these regeneration performance calculations assume 1) bidirectionally symmetric and constant (i.e., torque and velocity independent) actuator efficiencies, 2) losses only from the actuator-transmission system (i.e., Joule heating and friction), and 3) electrical regeneration over the entire negative joint mechanical power range. Tables 1 and 2 summarize the individual joint biomechanical energies during level-ground walking and stand-to-sit movements, respectively.

Table 1. Hip, knee, and ankle joint mechanical work per walking stride [12]. The results are averages across different subjects (n=19) and normalized to total body mass (J/kg). "Total Work" is the combined biomechanical energies from each joint and "Net Joint Work" is the net lower-limb joint mechanical work performed on the system.

	Positive Work	Negative Work	Net Joint Work
Hip Joint	0.130	-0.049	0.081
Knee Joint	0.074	-0.223	-0.149
Ankle Joint	0.313	-0.110	0.203
Total Work	0.517	-0.382	0.135

Table 2. Hip, knee, and ankle joint mechanical work per stand-to-sit movement. The results are averages across different subjects (n=9) and trials (20 trials/subject) and normalized to total body mass (J/kg). "Total Work" is the combined biomechanical energies from each joint and "Net Joint Work" is the net lower-limb joint mechanical work performed on the system.

	Positive Work	Negative Work	Net Joint Work
Hip Joint	0.038	-0.347	-0.309
Knee Joint	0.001	-0.147	-0.146
Ankle Joint	0.011	-0.022	-0.011
Total Work	0.050	-0.516	-0.466

Integrating the positive mechanical power curves in Fig. 1 provides insight into the energetic requirements (battery consumption) of robotic exoskeletons and prostheses during level-ground walking. Based on these calculations, human walking requires ~0.52 J/kg total positive lower-limb joint mechanical work per stride to generate forward propulsion, which equates to ~66 Joules of electrical energy, assuming an 80-kg user and the aforementioned regenerative powertrain system model. Using a single rechargeable lithium-ion battery (e.g., 2.6 Ah and 24 V with a total battery capacity of 224,640 Joules) [21], robotic exoskeletons and prostheses could theoretically walk ~3,404 steps per battery charge. The operating durations could therefore be extended by an additional ~40% (i.e., ~1,376 additional steps for 4,780 total steps) from energy regenerated during level-ground walking, and by an additional ~0.7% (i.e., ~24 additional steps for 3,428 total steps) from energy regenerated during stand-to-sit movements, assuming 60 repetitions per day [40]. In other words, level-ground walking and stand-to-sit movements could each regenerate ~64,676 Joules and ~1,560 Joules of total electrical energy per day, respectively. Here we assume sufficient power electronics to control the bidirectional flow of electrical power between the motor and onboard battery. Although electrical regeneration during level-ground walking can theoretically regenerate more energy than stand-to-sit movements over an extended period (i.e., assuming healthy biomechanical data and activity levels), there are projected advantages to energy regeneration from stand-to-sit movements, as subsequently discussed.

Control of regenerative actuators is notoriously challenging [5]. However, the actuator control during stand-to-sit movements would have higher tolerances to reference tracking errors since the joint biomechanical energies are almost entirely negative (see Fig. 7). In comparison, energy regeneration during level-ground walking would require more robust actuator control since the joint biomechanical energies are intermittent, multidirectional, and time-varying (see Fig. 1). Inaccurate and/or delayed reference tracking could result in regenerating energy during periods of positive mechanical work. Unlike regenerative braking, generating electricity from exerting positive mechanical work would require the human muscles to actively backdrive the actuator-transmission system, therein increasing the metabolic power consumption and decreasing the overall system efficiency [19]-[20], [25]-[26]. These energetic consequences are especially pertinent to aging and rehabilitation populations who already exhibit more inefficient walking [3]. There are advantages and disadvantages to energy regeneration from different human movements (e.g., stand-to-sit movements may regenerate less energy per day than level-ground walking, but can facilitate more robust reference tracking and control). For maximum efficiency and battery performance, robotic exoskeletons and prostheses should regenerate energy from many different negative mechanical work movements (i.e., walking, sitting down, and ramp and stair descent).

Our regeneration performance calculations were based on healthy young adults, therein requiring several assumptions and extrapolations to aging and rehabilitation populations. Healthy young adults have self-selected walking speeds ~1.35 m/s and walk between 6,000 and 13,000 steps/day [3]. In contrast, older adults typically walk slower and shorter distances. Approximately 50% of individuals over 65 years walk less than 5000 steps/day [3]. These activity levels are further diminished in persons with neuromusculoskeletal conditions. For instance, those with incomplete spinal cord injuries walk ~1,640 steps/day [3]. These population differences, especially in walking speed, have implications on regeneration performance. Empirical studies of robotic exoskeletons and prostheses with regenerative actuators have shown a positive correlation between walking speed and both electrical energy regeneration and efficiency (i.e., faster walking generates more electricity and more efficiently) [15]-[16], [21], [23], [25]-[26], [33]. For a given

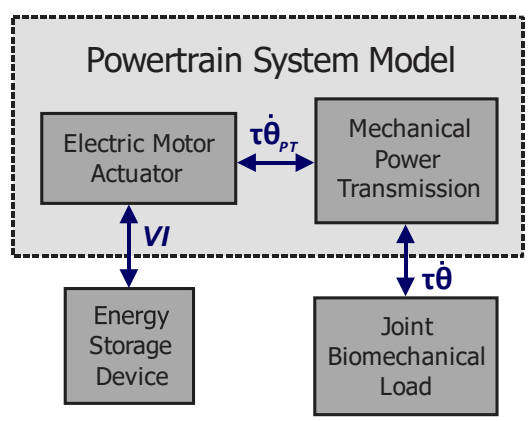

Fig. 8 Example of an exoskeleton/prosthesis powertrain system model, including an energy storage device, electric motor, mechanical power transmission (PT), and biomechanical load. The arrows represent the bidirectional flow of electrical (VI) and mechanical ($\tau\dot{\theta}$) power during motoring and generating operations.

back EMF constant, an electric motor generates a voltage proportional to rotational speed. Slower walking speeds would backdrive an electric motor with lower rotational speeds and therefore generate less electricity. Motors are also typically less efficient when generating torques at lower speeds due to Joule heating. For example, a recent study [33] showed that increasing walking speed from 0.9 m/s to 1.6 m/s increased power conversion efficiency from 40% to 59%. Taking into consideration the biomechanical and activity level differences between healthy young adults and mobility-impaired individuals, and the implications of such differences on energy regeneration and efficiency, future research should include seniors and/or rehabilitation patients to improve our regeneration performance calculations.

V. Conclusion

Regenerative actuators can extend the operating durations of robotic exoskeletons and prostheses by converting the otherwise dissipated joint biomechanical energy during negative work movements into electrical energy for battery recharging. However, previous research has focused exclusively on level-ground walking applications. Motivated by these limitations, we analyzed the lower-limb joint mechanical power during stand-to-sit movements using inverse dynamic simulations to estimate the biomechanical energy available for electrical regeneration. The hip produced the largest peak negative mechanical power (1.8 ± 0.5 W/kg), followed by the knee (0.8 ± 0.3 W/kg) and ankle (0.2 ± 0.1 W/kg). Negative mechanical work from the hip, knee, and ankle joints per stand-to-sit movement were 0.35 ± 0.06 J/kg, 0.15 ± 0.08 J/kg, and 0.02 ± 0.01 J/kg, respectively. Backdriving a modelled regenerative actuator on each lower-limb joint using these biomechanical inputs, robotic exoskeletons or prostheses could theoretically regenerate ~26 Joules of total electrical energy while sitting down, compared to ~19 Joules per walking stride. Given that these regeneration performance calculations were based on healthy young adults, future research should expand our analyses to include aging and/or rehabilitation populations to more accurately estimate the biomechanical energy available for electrical regeneration.

Acknowledgments

This research was funded by the Natural Sciences and Engineering Research Council of Canada (NSERC), the Waterloo Engineering Excellence PhD Fellowship program, and John McPhee's Tier I Canada Research Chair in Biomechatronic System Dynamics. We thank Stacey Acker (University of Waterloo, Canada) and Mark Charlet (Université Laval, Canada) for assisting with the biomechanical experiments.

References

[1] A. J. Young and D. P. Ferris, "State of the art and future directions for lower limb robotic exoskeletons," *IEEE Transactions on Neural Systems and Rehabilitation Engineering*, vol. 25, no. 2, pp. 171-182, 2017, DOI: 10.1109/TNSRE.2016.2521160.

[2] A. Maryniak, B. Laschowski, and J. Andrysek, "Technical overview of osseointegrated transfemoral prostheses: Orthopedic surgery and implant design centered," *ASME Journal of Engineering and Science in Medical Diagnostics and Therapy*, vol. 1, no. 2, pp. 020801-020801-7, 2018, DOI: 10.1115/1.4039105.

[3] M. Grimmer, R. Riener, C. J. Walsh, and A. Seyfarth, "Mobility related physical and functional losses due to aging and disease - A motivation for lower limb exoskeletons," *Journal of NeuroEngineering and Rehabilitation*, vol. 16, 2019, DOI: 10.1186/s12984-018-0458-8.

[4] B. Laschowski and J. Andrysek, "Electromechanical design of robotic transfemoral prostheses," *in Proceedings of the ASME International Design Engineering Technical Conferences and Computers and Information in Engineering Conference*, Quebec City, Canada, 2018, pp. V05AT07A054, DOI: 10.1115/DETC2018-85234.

[5] B. Laschowski, J. McPhee, and J. Andrysek, "Lower-limb prostheses and exoskeletons with energy regeneration: Mechatronic design and optimization review," *ASME Journal of Mechanisms and Robotics*, vol. 11, no. 4, pp. 040801-040801-8, 2019, DOI: 10.1115/1.4043460.

[6] D. S. Pieringer, M. Grimmer, M. F. Russold, and R. Riener, "Review of the actuators of active knee prostheses and their target design outputs for activities of daily living," *in Proceedings of the IEEE International Conference on Rehabilitation Robotics (ICORR),* London, UK, July 17-20, 2017, pp. 1246-1253, DOI: 10.1109/ICORR.2017.8009420.

[7] A. M. Simon, N. P. Fey, K. A. Ingraham, A. J. Young, and L. J. Hargrove, "Powered prosthesis control during walking, sitting, standing, and non-weight bearing activities using neural and mechanical inputs," *in Proceedings of the International IEEE/EMBS Conference on Neural Engineering (NER),* San Diego, USA, November 6-8, 2013, pp. 1174-1177, DOI: 10.1109/NER.2013.6696148.

[8] J. Skelton, S. K. Wu, and X. Shen, "Design of a powered lower-extremity orthosis for sit-to-stand and ambulation assistance," *ASME Journal of Medical Devices,* vol. 7, no. 3, pp. 030910-030910-2, 2013, DOI: 10.1115/1.4024489.

[9] S. Thapa, H. Zheng, G. F. Kogler, and X. Shen, "A robotic knee orthosis for sit-to-stand assistance," *in Proceedings of the ASME Dynamic Systems and Control Conference (DSCC)*, Minneapolis, USA, 2016, pp. V001T07A004, DOI: 10.1115/DSCC2016-9891.

[10] A. M. Dollar and H. Herr, "Active orthoses for the lower-limbs: Challenges and state of the art," *in Proceedings of the IEEE International Conference on Rehabilitation Robotics (ICORR)*, Noordwijk, Netherlands, June 13-15, 2017, pp. 968-977, DOI: 10.1109/ICORR.2007.4428541.

[11] A. M. Dollar and H. Herr, "Lower extremity exoskeletons and active orthoses: Challenges and state-of-the-art," *IEEE Transactions on Robotics*, vol. 24, no. 1, pp. 144-158, 2008, DOI: 10.1109/TRO.2008.915453.

[12] D. A. Winter, "*The Biomechanics and Motor Control of Human Gait: Normal, Elderly, and Pathological*," Waterloo Biomechanics, Canada, 1998.

[13] R. Razavian, N. L. Azad, and J. McPhee, "On real-time optimal control of a series hybrid electric vehicle with an ultra-capacitor," *in Proceedings of the American Control Conference (ACC)*, Montreal, Canada, June 27-29, 2012, pp. 547-552, DOI: 10.1109/ACC.2012.6314831.

[14] G. Rizzoni and H. Peng, "Hybrid and electrified vehicles: The role of dynamics and control," *ASME Mechanical Engineering Magazine*, vol. 135, no. 03, pp. S10-S17, 2012, DOI: 10.1115/1.2013-MAR-5.

[15] J. Andrysek and G. Chau, "An electromechanical swing-phase-controlled prosthetic knee joint for conversion of physiological energy to electrical energy: Feasibility study," *IEEE Transactions on Biomedical Engineering*, vol. 54, no. 12, pp. 2276-2283, 2007, DOI: 10.1109/TBME.2007.908309.

[16] J. Andrysek, T. Liang, and B. Steinnagel, "Evaluation of a prosthetic swing-phase controller with electrical power generation," *IEEE Transactions on Neural Systems and Rehabilitation Engineering*, vol. 17, no. 4, pp. 390-396, 2009, DOI: 10.1109/TNSRE.2009.2023292.

[17] T. Barto and D. Simon, "Neural network control of an optimized regenerative motor drive for a lower-limb prosthesis," *in Proceedings of the American Control Conference (ACC)*, Seattle, USA, May 24-26, 2017, pp. 5330-5335, DOI: 10.23919/ACC.2017.7963783.

[18] E. Bolivar, S. Rezazadeh, and R. Gregg, "A general framework for minimizing energy consumption of series elastic actuators with regeneration," *in Proceedings of the ASME Dynamic Systems and Control Conference (DSCC)*, Tysons, USA, 2017, pp. V001T36A005, DOI: 10.1115/DSCC2017-5373.

[19] J. M. Donelan, Q. Li, V. Naing, J. A. Hoffer, D. J. Weber, and A. D. Kuo, "Biomechanical energy harvesting: Generating electricity during walking with minimal user effort," *Science*, vol. 319, no. 5864, pp. 807-810, 2008, DOI: 10.1126/science.1149860.

[20] J. M. Donelan, V. Naing, and Q. Li, "Biomechanical energy harvesting," *in Proceedings of the IEEE Radio and Wireless Symposium*, San Diego, USA, January 18-22, 2009, pp. 1-4, DOI: 10.1109/RWS.2009.4957269.

[21] Y. Feng, J. Mai, S. K. Agrawal, and Q. Wang, "Energy regeneration from electromagnetic induction by human dynamics for lower extremity robotic prostheses," *IEEE Transactions on Robotics*, 2020, DOI: 10.1109/TRO.2020.2991969.

[22] E. Gualter Dos Santos and H. Richter, "Modeling and control of a novel variable-stiffness regenerative actuator," *in Proceedings of the ASME Dynamic Systems and Control Conference (DSCC)*, Atlanta, USA, 2018, pp. V002T24A003, DOI: 10.1115/DSCC2018-9054.

[23] P. Khalaf, H. Warner, E. Hardin, H. Richter, and D. Simon, "Development and experimental validation of an energy regenerative prosthetic knee controller and prototype," *in Proceedings of the ASME Dynamic Systems and Control Conference (DSCC)*, Atlanta, USA, 2018, pp. V001T07A008, DOI: 10.1115/DSCC2018-9091.

[24] B. H. Kim and H. Richter, "Energy regeneration-based hybrid control for transfemoral prosthetic legs using four-bar mechanism," *in Proceedings of the Annual Conference of the IEEE Industrial Electronics Society*, Washington, USA, October 21-23, 2018, pp. 2516-2521, DOI: 10.1109/IECON.2018.8591399.

[25] Q. Li, V. Naing, J. A. Hoffer, D. J. Weber, A. D. Kuo, and J. M. Donelan, "Biomechanical energy harvesting: Apparatus and method," *in Proceedings of the IEEE International Conference on Robotics and Automation (ICRA),* Pasadena, USA, May 19-23, 2008, pp. 3672-3677, DOI: 10.1109/ROBOT.2008.4543774.

[26] Q. Li, V. Naing, and J. M. Donelan, "Development of a biomechanical energy harvester," *Journal of NeuroEngineering and Rehabilitation*, vol. 6, no. 22, 2009, DOI: 10.1186/1743-0003-6-22.

[27] R. Rarick, H. Richter, A. Van Den Bogert, D. Simon, H. Warner, and T. Barto, "Optimal design of a transfemoral prosthesis with energy storage and regeneration," *in Proceedings of the American Control Conference (ACC)*, Portland, USA, June 4-6, 2014, pp. 4108-4113, DOI: 10.1109/ACC.2014.6859051.

[28] F. Rohani, H. Richter, and A. J. Van Den Bogert, "Optimal design and control of an electromechanical transfemoral prosthesis with energy regeneration," *PLoS ONE*, vol. 12, no. 11, pp. e0188266, 2017, DOI: 10.1371/journal.pone.0188266.

[29] M. R. Tucker and K. B. Fite, "Mechanical damping with electrical regeneration for a powered transfemoral prosthesis," *in Proceedings of the IEEE/ASME International Conference on Advanced Intelligent Mechatronics*, Montreal, Canada, July 6-9, 2010, pp. 13-18, DOI: 10.1109/AIM.2010.5695828.

[30] H. Warner, D. Simon, and H. Richter, "Design optimization and control of a crank-slider actuator for a lower-limb prosthesis with energy regeneration," *in Proceedings of the IEEE International Conference on Advanced Intelligent Mechatronics*, Banff, Canada, July 12-15, 2016, pp. 1430-1435, DOI: 10.1109/AIM.2016.7576971.

[31] E. Bolivar, S. Rezazadeh, and R. D. Gregg, "Minimizing energy consumption and peak power of series elastic actuators: A convex optimization framework for elastic element design," *IEEE/ASME Transactions on Mechatronics*, vol. 24, no. 3, pp. 1334-1345, 2019, DOI: 10.1109/TMECH.2019.2906887.

[32] T. Elery, S. Rezazadeh, C. Nesler, J. Doan, H. Zhu, and R. D. Gregg, "Design and benchtop validation of a powered knee-ankle prosthesis with high-torque, low-impedance actuators," *in Proceedings of the IEEE International Conference on Robotics and Automation (ICRA)*, Brisbane, QLD, Australia, May 21-25, 2018, DOI: 10.1109/ICRA.2018.8461259.

[33] T. Elery, S. Rezazadeh, C. Nesler, and R. Gregg, "Design and validation of a powered knee-ankle prosthesis with high-torque, low-impedance actuators," *IEEE Transactions on Robotics*, 2020, DOI: 10.1109/TRO.2020.3005533.

[34] G. Lv, H. Zhu, and R. D. Gregg, "On the design and control of highly backdrivable lower-limb exoskeletons: A discussion of past and ongoing work," *IEEE Control Systems Magazine*, vol. 38, no. 6, pp. 88-113, 2018, DOI: 10.1109/MCS.2018.2866605.

[35] H. Zhu, J. Doan, C. Stence, G. Lv, T. Elery, and R. Gregg, "Design and validation of a torque dense, highly backdrivable powered knee-ankle orthosis," *in Proceedings of the IEEE International Conference on Robotics and Automation (ICRA)*, Singapore, May 29 - June 3, 2017, DOI: 10.1109/ICRA.2017.7989063.

[36] H. Zhu, C. Nesler, N. Divekar, M. Taha Ahmad, and R. D. Gregg, "Design and validation of a partial-assist knee orthosis with compact, backdrivable actuation," *in Proceedings of the IEEE International Conference on Rehabilitation Robotics (ICORR),* Toronto, ON, Canada, June 24-28, 2019, DOI: 10.1109/ICORR.2019.8779479.

[37] G. Khademi, H. Richter, and D. Simon, "Multi-objective optimization of tracking/impedance control for a prosthetic leg with energy regeneration," *in Proceedings of the IEEE Conference on Decision and Control*, Las Vegas, USA, December 12-14, 2016, pp. 5322-5327, DOI: 10.1109/CDC.2016.7799085.

[38] G. Khademi, H. Mohammadi, H. Richter, and D. Simon, "Optimal mixed tracking/impedance control with application to transfemoral prostheses with energy regeneration," *IEEE Transactions on Biomedical Engineering*, vol. 65, no. 4, pp. 894-910, 2018, DOI: 10.1109/TBME.2017.2725740.

[39] R. Riemer and A. Shapiro, "Biomechanical energy harvesting from human motion: Theory, state of the art, design guidelines, and future directions," *Journal of NeuroEngineering and Rehabilitation*, pp. 22, 2011, DOI: 10.1186/1743-0003-8-22.

[40] A. M. Simon, N. P. Fey, K. A. Ingraham, S. B. Finucane, E. G. Halsne, and L. J. Hargrove, "Improved weight-bearing symmetry for transfemoral amputees during standing up and sitting down with a powered knee-ankle prosthesis," *Archives of Physical Medicine and Rehabilitation*, vol. 97, no. 7, pp. 1100-1106, 2016, DOI: 10.1016/j.apmr.2015.11.006.

[41] F. Gao, F. Zhang, and H. Huang, "Investigation of sit-to-stand and stand-to-sit in an above knee amputee," *in Proceedings of the Annual International Conference of the IEEE Engineering in Medicine and Biology Society (EMBC)*, Boston, USA, August 30 - September 3, 2011, pp. 7340-7343, DOI: 10.1109/IEMBS.2011.6091712.

[42] M. K. Shepherd and E. J. Rouse, "Design and characterization of a torque-controllable actuator for knee assistance during sit-to-stand," *in Proceedings of the Annual International Conference of the IEEE Engineering in Medicine and Biology Society (EMBC)*, Orlando, USA, August 16-20, 2016, pp. 2228-2231, DOI: 10.1109/EMBC.2016.7591172.

[43] M. K. Shepherd and E. J. Rouse, "Design and validation of a torque-controllable knee exoskeleton for sit-to-stand assistance," *IEEE/ASME Transactions on Mechatronics*, vol. 22, no. 4, pp. 1695-1704, 2017, DOI: 10.1109/TMECH.2017.2704521.

[44] J. Vantilt, K. Tanghe, M. Afschrift, A. Bruijnes, K. Junius, J. Geeroms, E. Aertbeliën, F. De Groote, D. Lefeber, I. Jonkers, and J. De Schutter, "Model-based control for exoskeletons with series elastic actuators evaluated on sit-to-stand movements," *Journal of NeuroEngineering and Rehabilitation*, vo. 16, pp. 65, 2019, DOI: 10.1186/s12984-019-0526-8.

[45] H. A. Varol, F. Sup, and M. Goldfarb, "Powered sit-to-stand and assistive stand-to-sit framework for a powered transfemoral prosthesis," *in Proceedings of the IEEE International Conference on Rehabilitation Robotics (ICORR),* Kyoto, Japan, June 23-26, 2009, pp. 645-651, DOI: 10.1109/ICORR.2009.5209582.

[46] M. Wu, M. R. Haque, and X. Shen, "Sit-to-stand control of powered knee prostheses," *in Proceedings of the ASME Design of Medical Devices Conference*, Minneapolis, USA, 2017, pp. V001T05A015, DOI: 10.1115/DMD2017-3507.

[47] R. S. Razavian, S. Greenberg, and J. McPhee, "Biomechanics Imaging and Analysis," *Encyclopedia of Biomedical Engineering*, pp. 488-500, 2019, DOI: 10.1016/B978-0-12-801238-3.99961-6.

[48] S. L. Delp, et al., "OpenSim: Open-source software to create and analyze dynamic simulations of movement," *IEEE Transactions on Biomedical Engineering*, vol. 54, no. 11, pp. 1940-1950, 2007, DOI: 10.1109/TBME.2007.901024.

[49] A. J. van den Bogert and A. Su, "A weighted least squares method for inverse dynamic analysis," *Computer Methods in Biomechanics and Biomedical Engineering*, vol. 11, no. 1, pp. 3-9, 2008, DOI: 10.1080/10255840701550865.

[50] B. Laschowski and J. McPhee, "Body segment parameters of Paralympic athletes from dual-energy X-ray absorptiometry," *Sports Engineering*, vol. 19, no. 3, pp. 155-162, 2016, DOI: 10.1007/s12283-016-0200-3.

[51] B. Laschowski and J. McPhee, "Quantifying body segment parameters using dual-energy X-ray absorptiometry: A Paralympic wheelchair curler case report," *Procedia Engineering*, vol. 147, pp. 163-167, 2016, DOI: 10.1016/j.proeng.2016.06.207.

[52] P. De Leva, "Adjustments to Zatsiorsky-Seluyanov's segment inertia parameters," *Journal of Biomechanics*, vol. 29, no. 9, pp. 1223-1230, 1996, DOI: 10.1016/0021-9290(95)00178-6.

[53] S. Seok, A. Wang, M. Y. Chuah, D. Otten, J. Lang, and S. Kim, "Design principles for highly efficient quadrupeds and implementation on the MIT cheetah robot," *in Proceedings of the IEEE International Conference on*

Robotics and Automation, Karlsruhe, Germany, May 6-10, 2013, DOI: 10.1109/ICRA.2013.6631038.

[54] S. Seok, A. Wang, M. Y. Chuah, D. J. Hyun, J. Lee, D. M. Otten, J. H. Lang, and S. Kim, "Design principles for energy-efficient legged locomotion and implementation on the MIT cheetah robot," *IEEE/ASME Transactions on Mechatronics*, vol. 20, no. 3, pp. 1117-1129, 2015, DOI: 10.1109/TMECH.2014.2339013.